Ordered Nanostructures Self-Assembled from Block Copolymer Tethered Nanoparticles

Xiaomeng Zhu, Liquan Wang, Jiaping Lin,* and Liangshun Zhang

Shanghai Key Laboratory of Advanced Polymeric Materials, Key Laboratory for Ultrafine Materials of Ministry of Education, School of Materials Science and Engineering, East China University of Science and Technology, Shanghai 200237, China

ARTICLE

ABSTRACT Combining the self-consistent field theory (SCFT) and the density functional theory (DFT), we investigated the self-assembly behavior of AB diblock copolymer tethered single spherical particle P (ABP molecules). Two cases were studied: one is where the particles are chemically neutral to both A and B blocks, and the other is where the particles are unfavorable to neither of the two blocks. For neutral particles, the ABP molecules self-assemble to typical equilibrium microstructures, such as lamellae and cylinders. The P particles are localized in B block domains, and the size of particles can influence the phase behavior. For unfavorable particles, the ABP molecules microphase separate to form distinct ordered structures. Hierarchical structures, such as cylinders with cylinders at the interfaces and lamellae with cylinders at the interfaces, were observed. These resulting hierarchical structures are mainly determined by two parameters: A block fraction f_A and particle size R_P. On the basis of the calculation results, phase diagrams were constructed.

KEYWORDS: self-assembly · hierarchical structures · nanoparticles · diblock copolymer · self-consistent field theory

Self-assembly is the promising means for designing and controlling assembly of nanoparticles into highly ordered structures for applications of biosensors, energy storage, and electronic devices.[1−4] Soft matter such as block copolymers can form various ordered structures, such as lamellae, cylinders, and spheres, providing a template for nanoparticle distribution.[5−9] Connecting coil polymer tethers to the nanoparticles provides an alternative opportunity for creating nanoparticle/polymer assembly with enhanced properties. By designing the architecture of molecules, the polymer tethered nanoparticle can produce novel complex self-assembled nanostructures. The overall morphology is affected not only by the asymmetry of the molecule architecture but also by the size and shape of the nanoparticle.[10,11] Due to the complexity of these polymer tethered nanoparticle systems, understanding the phase behavior of the polymer tethered nanoparticle presents a challenge.

To control nanoparticle assembly for designing new nanomaterials, the phase behaviors of various typical polymer tethered nanoparticles were investigated by researchers. In practice, inorganic and metal nanoparticles (*e.g.*, Si, Au, Ag, CdTe, *etc.*) are utilized to be connected with various types of polymer tethers. For example, polystyrene attached gold nanoparticles can self-assemble into hexagonally packed ordered structure with tenability of the optical properties.[12] In addition, organic nanoparticles, for instance, polyhedral oligmeric silsesquioxane (POSS) molecules, have been prepared as a class of cubic-shaped nanobuilding blocks which can also be used to construct advanced nanomaterials.[13,14] Drazkowski *et al.* prepared a sample of styrene−butadiene−styrene triblock copolymer tethered with isobutyl-substituted POSS.[15] It was found that the self-assembly of the copolymer can be tuned by the nanoparticles. Inversely, the self-assembly of the copolymer can also direct the spatial distribution of the nanoparticles in the polymer matrix.

Although there are many experimental studies of polymer tethered nanoparticle assemblies in the literature, limited theoretical approaches are available, which can offer a comprehensive, predictable, and generally applicable scheme. Several theoretical and simulation tools, such as molecular Brownian dynamics,[16,17] Monte Carlo,[18] dissipative particle dynamics,[19−21] and self-consistent field theory,[22−31] have been used to study the self-assembled structures of tethered nanoparticles. Glotzer *et al.* utilized molecular Brownian dynamics simulation to investigate the self-assembly of monotethered nanospheres, nanorods, nanocubes, and nanodisks.[10,16,32−34] A variety of nanostructures including lamellae, perforated lamellae, icosahedral, and

*Address correspondence to jlin@ecust.edu.cn.

Received for review October 19, 2009 and accepted August 04, 2010.

Published online August 19, 2010. 10.1021/nn101121n

hexagonal packed cylinders were observed. These ordered morphologies depend on many factors, such as particle size, volume fraction, tether chemistry, and intermolecular interactions. Theoretically, Schweizer *et al.* generalized a microscopic polymer reference interaction site model theory to study self-assembly behaviors of dense solutions or melts of spherical nanoparticles carrying different numbers of coil tethered chains.[35,36] It was found that the interplay of entropic and enthalpic effects results in different real-space structural arrangements. Despite these simulation and theoretical studies, much of the space of complex assemblies of polymer tethered nanoparticles still remains unexplored.

The real-space self-consistent field theory (SCFT) is a powerful technique for discovering the structures of complex architecture copolymers both in bulk and in solution.[37−43] In the real-space SCFT, a prior assumption about the asymmetry is not necessary. This method is found to be an efficient way to tackle the problem that the structure is unknown prior. Combining a self-consistent field theory (SCFT) for a polymer with a density functional theory (DFT) for particles, it is suitable to explore the self-assembly behavior of the polymer/nanoparticle systems.[44,45] Balazs *et al.* first developed this model (combination of SCFT and DFT) to investigate the phase behavior of mixtures of nanoparticle and diblock copolymers.[46,47] They also first extended the SCFT/DFT method to study a system of "tadpole" copolymers with spherical nanoparticle headgroup and a flexible polymer tail (AB tadpole).[48] It was found that AB tadpoles with nearly equal composition (55% A block and 45% B particle) can self-assemble into a hexagonally close-packed cylinder rather than alternating lamellae formed by AB diblock copolymers with the corresponding composition. The period is smaller in the tadpole system due to the steric interactions and packing constraints. Experimental studies confirmed that the "SCFT/DFT" prediction is very successful.[46−48] We utilized SCFT/DFT methodology to investigate the self-assembly behavior of the block copolymer/nanoparticle mixture in solution and alternating block copolymer/nanoparticle mixture in bulk.[9,49] The mixtures were found to be able to self-associate into various nanostructures with controllable size and morphology. So far, only limited studies of polymer tethered nanoparticles are available, and many issues remain to be solved.

Motivated by these successful SCFT/DFT predictions mentioned above and unsolved problems remaining in the self-assembly of polymer tethered nanoparticles, we carried out a systematic investigation of the phase behavior of AB diblock copolymer tethered single nanoparticle P with different chemical compatibility by using the SCFT/DFT method.

RESULTS AND DISCUSSION

In the present work, we assume that the system is incompressible with a total volume V, which contains n ABP macromolecules. Each molecule consists of an AB diblock copolymer chain which is attached to a spherical hard particle P with radius R_P. The variable f denotes the volume fraction of the AB diblock copolymer chain, and f_A is the fraction of A block within the diblock copolymer.

To simplify the studies, the interaction strength between A and B blocks is fixed to be $\chi_{AB}N = 30.0$. The P particles are chosen to be nonselective to A and B blocks, that is, $\chi_{AP}N = \chi_{BP}N$. Two types of tethered nanoparticles are studied here: (1) particles are neutral to both A and B blocks, where the interaction parameters are set to be $\chi_{AP}N = \chi_{BP}N = 0.0$; and (2) particles are unfavorable to both A and B blocks, where the interaction parameters are $\chi_{AP}N = \chi_{BP}N = 30.0$.

Neutral Particles. In this subsection, we studied the equilibrium microstructures self-assembled from the ABP macromolecules at $\chi_{AP}N = \chi_{BP}N = 0.0$. In this case, typical equilibrium morphologies, such as lamella (**L**) and cylinder (**C**), are observed. Figure 1 shows the obtained results of ABP macromolecules with neutral tethered particles at different values of f_A. The size of particles is fixed at $R_P/R_g = 0.33$. When the A block volume fraction f_A is 0.35, the ABP macromolecules self-assemble into the hexagonally packed cylindrical microstructure, as shown in Figure 1a. When f_A becomes 0.65, the lamellar structure is formed instead, which is shown in Figure 1b. To further understand the detailed structures, we plot the one-dimensional density profiles respectively for the A blocks, B blocks, and tethered P naoparticles. As can be seen from one-dimensional density profiles for cylinders in Figure 1c and lamellae in Figure 1d, the particles are mainly localized in the B domains, despite their nonselective particle−polymer interaction. This result implies that the nanoparticles act as one portion of B blocks.

The reason that the nonselective nanoparticles are confined in B domains rather than distributed uniformly over both A and B domains arises from the interplay of enthalpic and entropic effects. If nanoparticles are uniformly distributed in both A and B domains, the B segments are forced to be located in immiscible A domains owing to the chain connection between particles and the end of B blocks. Thus, the interaction energy between A and B blocks increases. To prove this argument being correct, the free-energy contributions of microstructures with nanoparticles in the B domain and uniformly distributed in A and B domains were calculated. The total free energy is decomposed into interaction energy U and contribution of conformational entropy $-TS$. The results are presented in Table 1. As can be seen, the interaction energy is lower but the loss of conformational entropy of ABP macromolecules is greater in the case of nanoparticles in the B domain

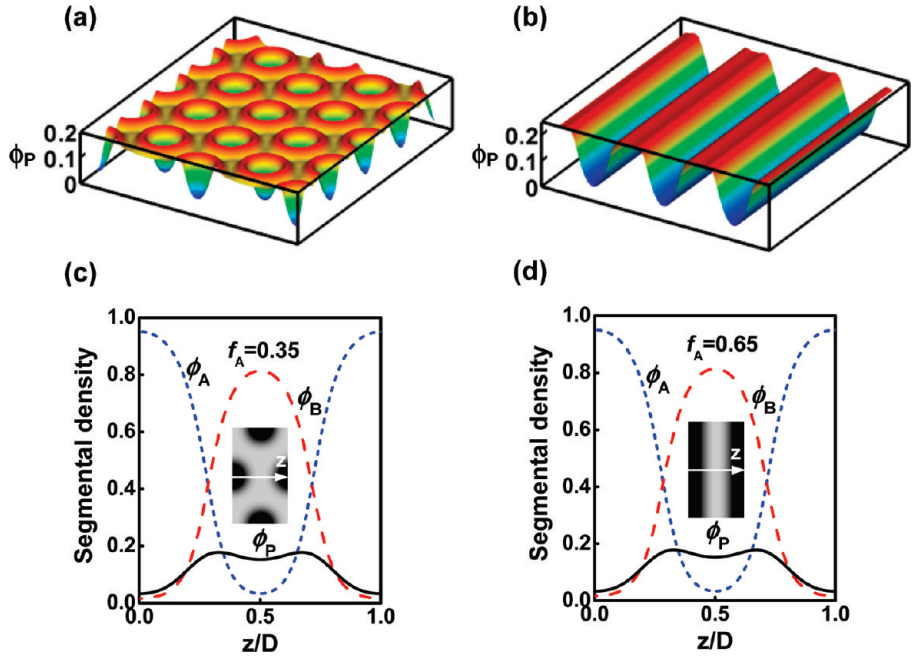

Figure 1. Nanoparticle density profiles from SCFT/DFT for ABP macromolecules with $\chi_{AB}N = 30.0$, $\chi_{AP}N = \chi_{BP}N = 0.0$, and $R_P/R_g = 0.33$ at different values of f_A: (a) 0.35 and (b) 0.65. Red represents high local volume fraction of particles, while blue indicates low local volume fraction of particles. One-dimensional density profiles of blocks A, blocks B, and nanoparticles P are shown in (c) and (d) correspondingly. The insets of (c) and (d) show the spatial coordinate *z* in units of domain spacing *D* marked with an arrow.

relative to the corresponding values for the case of nanoparticles uniformly distributed in A and B domains. Although the entropic loss is lower in uniformly distributed particle systems, it is not enough to compensate the increase in interaction enthalpy. As a result, nanoparticles are preferable to be localized in B domains due to the lower total free energy.

Summarizing the simulation results for the neutral tethered nanoparticles with $R_P/R_g = 0.33$ at various values of interaction strength and A block volume fraction, we plot the phase diagram in $\chi_{AB}N-f_A$ space. The phase diagram is illustrated in Figure 2. Each point in the phase diagram corresponds to a simulation result, and lines are drawn to identify the resulting phase boundaries. The phase diagram contains four characteristic zones: disorder state (**Dis**), hexagonally packed cylinders occupied by A blocks ($\mathbf{C}_A$), hexagonally packed cylinders occupied by B blocks ($\mathbf{C}_B$), and lamellae (**L**). The $\mathbf{C}_A$ structures are found to exist in a wider range of the diagram. Meanwhile, the region representing the $\mathbf{C}_B$ structures is relatively narrower. According to the analysis of energy contribution, which is mentioned above, the nanoparticles always prefer the B domains. The lamellae prefer to be formed at large values of f_A. For example, when $\chi_{AB}N = 20$, **L** is observed at $f_A = 0.6$ while $\mathbf{C}_A$ is formed at $f_A = 0.4$, as shown in Figure 2. It is also noted that this phase diagram is not symmetrical about $f_A = 0.5$.

We further studied the effect of nanoparticle size on the phase behaviors. The results are summarized into a phase diagram in the space of R_P/R_g-f_A, as shown in Figure 3. In the phase diagram, the region of or-

TABLE 1. Comparison of Total Free Energy *F*, Interaction Energy *U*, and Contribution of Conformational Entropy $-TS$ of ABP Macromolecuels for the Localization of Nanoparticles in B Block Domains and Uniformly over A and B Block Domains at $\chi N_{AB} = 30.0$, $\chi N_{AP} = \chi N_{BP} = 0.0$ and $f_A = 0.65$

	nanoparticles localized in B block domains	nanoparticles distributed uniformly over A and B block domains
F	3.505	3.870
U	2.319	3.418
$-TS$	1.186	0.452

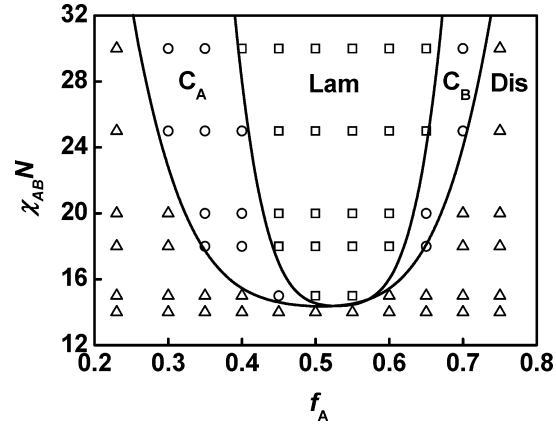

Figure 2. Phase diagram in $\chi_{AB}N-f_A$ space for ABP macromolecules with $\chi_{AP}N = \chi_{BP}N = 0.0$ and $R_P/R_g = 0.33$. Dis labels the regions where the melt is disordered. The ordered regions include $\mathbf{C}_A$ (cylinder domains formed by A blocks), Lam (lamellae), and $\mathbf{C}_B$ (cylinder domains formed by B blocks). In this diagram, the phase boundaries are drawn to guide the eye based on the calculated points.

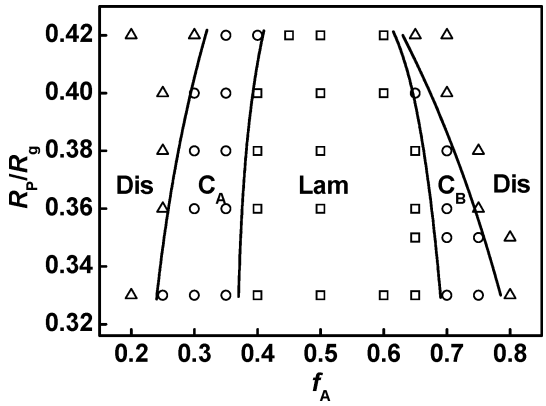

Figure 3. Phase diagram in R_P/R_g-f_A space for ABP macromolecules with $\chi_{AB}N = 30.0$ and $\chi_{AP}N = \chi_{BP}N = 0.0$. Labels appear as in Figure 2.

dered phase becomes narrow as R_P/R_g increases. In addition, an increase in value of R_P/R_g shrinks the phase regions of $\mathbf{C}_A$, **L**, and $\mathbf{C}_B$, where the phase boundaries of order−order transitions shift toward larger f_A values when $f_A < 0.5$ and lower f_A values when $f_A > 0.5$. The stable ordered phase of $\mathbf{C}_A$, where the B blocks form the majority domains, is broader than those of reverse phase $\mathbf{C}_B$. These results indicate that the nanoparticle size has a profound effect on the self-assembled nanostructures in this ABP macromolecule system.

It is difficult to make a quantitative comparison between the theoretical predications and experimental observations due to few experiments on AB copolymer tethered nanoparticles in the literature. However, we can qualitatively compare the calculation results with some existing experimental studies on the systems of copolymer tethered nanoparticles. For example, Drazkowski *et al.* investigated the self-assembly of the triblock polystyrene−butadiene−polystyrene (SBS) copolymer tethered with isobutyl-substituted polyhedral oligomeric silsesquioxane (POSS) molecules.[15] It was found that the SBS-POSS macromolecules can form the lamellar or cylindrical nanostructures. The POSS is confined within the polybutadiene domain. Furthermore, with an increase in POSS content at fixed polymer content, phase transition from lamella to cylinder takes place for the tethered SBS copolymer. In our simulations, lamellar and cylindrical structures are observed. In both nanostructures, the neutral tethered nanoparticles, which can be regarded as POSS, are confined in block B domains (as shown in Figure 1c,d). In addition, we found a transition from lamella to cylinder with the increase of nanoparticles radius R_P/R_g, as shown in Figure 3. The increase in R_P/R_g can be regarded as an increase in POSS content. Such kinds of phase behaviors (*i.e.*, localization of nanoparticles in one block domains and lamella → cylinder transition induced by increase in R_P/R_g) are consistent with the experimental observations.

Unfavorable Particles. In this subsection, the nanoparticles are chosen to be chemically unfavorable to both A and B blocks. Under such circumstance, the interaction strengths between the P particles and the A and B blocks are set as $\chi_{AP}N = \chi_{BP}N = 30.0$.

Figure 4 shows the equilibrium morphologies obtained for ABP macromolecules with various values of f_A at $R_P/R_g = 0.4$. The green, blue, and red colors represent the domains rich in P particles, A blocks, and B blocks, respectively. When $f_A = 0.2$, as shown in Figure 4a, a hexagonally packed cylindrical phase ($\mathbf{C}_P$) is observed. In such a microstructure, the hexagonally packed cylindrical nanoparticle domains are isolated in the matrix formed by A and B blocks (blocks A and B are mixed). The AB tethers behave much like homopolymer tails, and the A and B blocks are not microphase-separated. The phase behavior of such ABP macromolecules shows similarity to that of AB tadpoles.[48] However, at the intermediate value of A block volume fractions, A and B blocks become phase-separated, thereby producing a series of complex structures which are not observed in the AB tadpole system. These structures exhibit hierarchical characteristics and have two different periods related to the two intrinsic length scales. Taking Figure 4b as an example, hierarchically ordered structures are formed from the ABP macromolecules when $f_A = 0.4$. The A blocks and BP blocks separate to form the hexagonally packed cylindrical patterns as the large-length-scale structure, and the nanoparticles form the squarely arranged cylindrical domains within the B block domains as the small-length-scale structure. We refer to such hierarchical structure as cylinders with nanoparticle cylinders at the interfaces ($\mathbf{C}_P$-in-**C**). Furthermore, when $f_A = 0.6$, alternating lamellar structures (large-length-scale period) are formed from the separation of A blocks and BP blocks, and the nanoparticles form the cylinders (small-length-scale period) at the interfaces (Figure 4c). When $f_A = 0.8$, lamellar structures (large-length-scale period) can be formed but with the cylinders of nanoparticles at the interior of B domains (small-length-scale period), as shown in Figure 4d. We define these structures as lamellae with nanoparticle cylinders at the interfaces ($\mathbf{C}_P$-in-$\mathbf{L}^{I}$) and lamellae with nanoparticle cylinders inside a domain ($\mathbf{C}_P$-in-$\mathbf{L}^{II}$), respectively. When $f_A = 0.9$, the $\mathbf{C}_P$ phases are found again, as shown in Figure 4e. In this microstructure, the hexagonally packed cylindrical nanoparticle domains are formed and the matrix consists of mixed blocks A and B. From the above results, it can be seen that, when the composition of A block is comparable to that of B block, the A and B blocks are phase-separated. Hierarchical ordered nanostructures appear. These nanostructures are different from those formed by AB tadpoles.[48] Such differences originate from the molecular architecture and chemical compatibility. Regarding all of the hierarchical structures, the large-length-scale assembly is attributed to phase separation between A blocks and BP blocks and the small-length-scale ordering is driven by the segregation between P nanoparticles and B blocks.

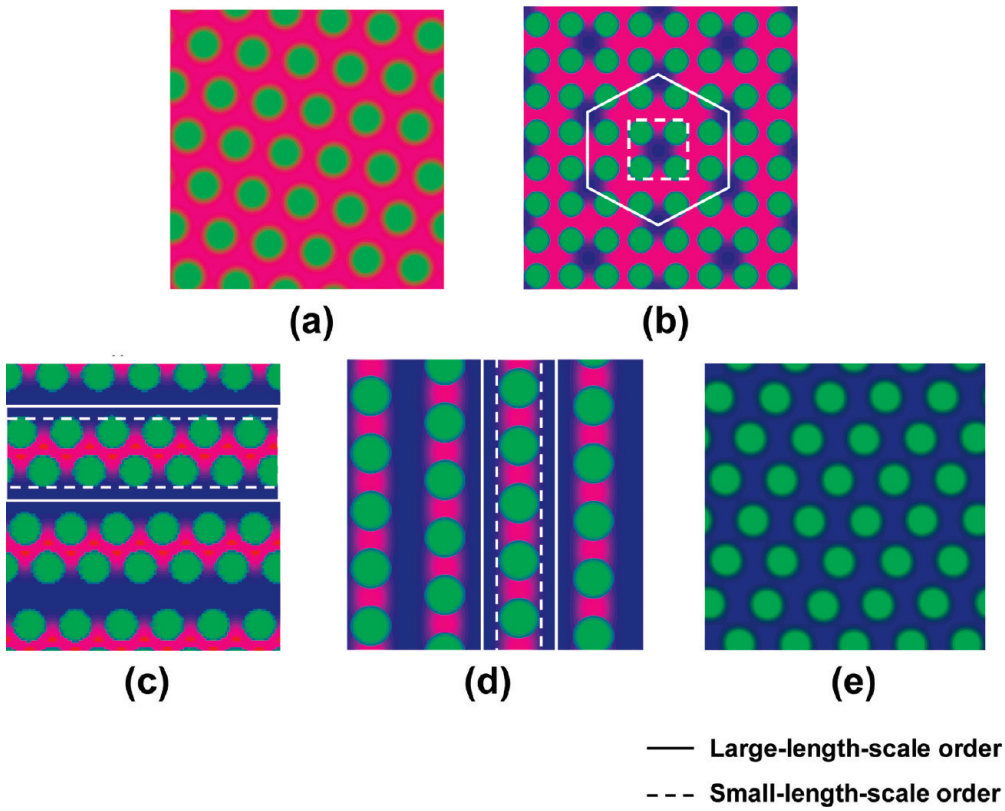

Figure 4. Ordered nanostructures self-assembled from ABP macromolecules with various A block volume fractions: (a) cylinders whose minority domains are occupied by nanoparticles ($\mathbf{C}_P$), $f_A = 0.2$; (b) cylinders with nanoparticle cylinders at the interfaces ($\mathbf{C}_P$-in-$\mathbf{C}$), $f_A = 0.4$; (c) lamellae with nanoparticle cylinders at the interfaces ($\mathbf{C}_P$-in-$\mathbf{L}^I$), $f_A = 0.6$; (d) lamellae with nanoparticle cylinders inside the domain ($\mathbf{C}_P$-in-$\mathbf{L}^{II}$), $f_A = 0.8$; (e) cylinders ($\mathbf{C}_P$), $f_A = 0.9$. The parameters are $R_P/R_g = 0.4$ and the Flory−Huggins interaction parameters $\chi_{AB}N = \chi_{AP}N = \chi_{BP}N = 30.0$. The blue, red, and green colors are assigned to A blocks, B blocks, and P particles, respectively.

The nanoparticle size is another impact factor which influences the resulting morphologies. For the ABP macromolecules containing small nanoparticles, the microphase separation between P nanoparticles and AB copolymer tethers does not occur. The P particles act as a part of B blocks. When the particles become larger, cylinders formed by nanoparticles can be observed at the fixed values of the A block volume fraction. We take the structure formed at $f_A = 0.8$ as an example to illustrate the effect of particle size on the phase behavior of the ABP macromolecules. In Figure 5, two-dimensional density profiles are plotted. The blue, red, and green colors denote the domains formed by A blocks, B blocks, and P nanoparticles, respectively. With increased particles radius, various types of morphologies can be observed as follows: hexagonally arranged cylindrical $\mathbf{C}_B$ phase at $R_P/R_g = 0.33$ (Figure 5a1), hierarchical structure $\mathbf{C}_P$-in-$\mathbf{L}^{II}$ at $R_P/R_g = 0.4$ (Figure 5b1), and hexagonally arranged cylindrical $\mathbf{C}_P$ phase at $R_P/R_g = 0.42$ (Figure 5c1). To further understand the detailed structure, we plot the one-dimensional density profiles of the A blocks (ϕ_A), B blocks (ϕ_B), P particles (ϕ_P), and particle centers (ρ_P) for corresponding structures, respectively, as shown in Figure 5a2−c2. In Figure 5a2, the profiles ϕ_B and ϕ_P show that the density distribution of particles is in the B block domains. This indicates that the small tethered particles are mixed with B blocks. The particles are forced near the AB interface as indicated by the particle center distribution ρ_P. In Figure 5b2, the cylindrical domains occupied by the nanoparticles emerge and the A and B blocks form the polymer matrix. With increased R_P/R_g, the nanoparticle cylinders are still available and the polymer matrixes are occupied mainly by the A blocks, as can be seen in Figure 5c2. In both Figure 5b2,c2, the particle center profile ρ_P reveals that the particles are localized at the center of cylindrical domains.

As shown in Figure 5, the hierarchical nanostructures formed by ABP macromolecules show a peculiar feature that the large tethered nanoparticles have a preference to aggregate to form the cylindrical domains. To demonstrate this process, a cartoon is presented in Figure 6. The blue, red, and green regions denote the A block domains, B block domains, and P particle domains, respectively. The possible molecule organizations, based on SCFT calculations, in these nanostructures are presented. The blue lines, red lines, and green spheres, respectively, represent the A blocks, B blocks, and P particles. When the tethered nanoparticles are small, for example, at $f_A = 0.8$, the hexagonally packed cylindrical structures are observed, as shown in Figure 6a. The cylindrical domains are occupied by the B

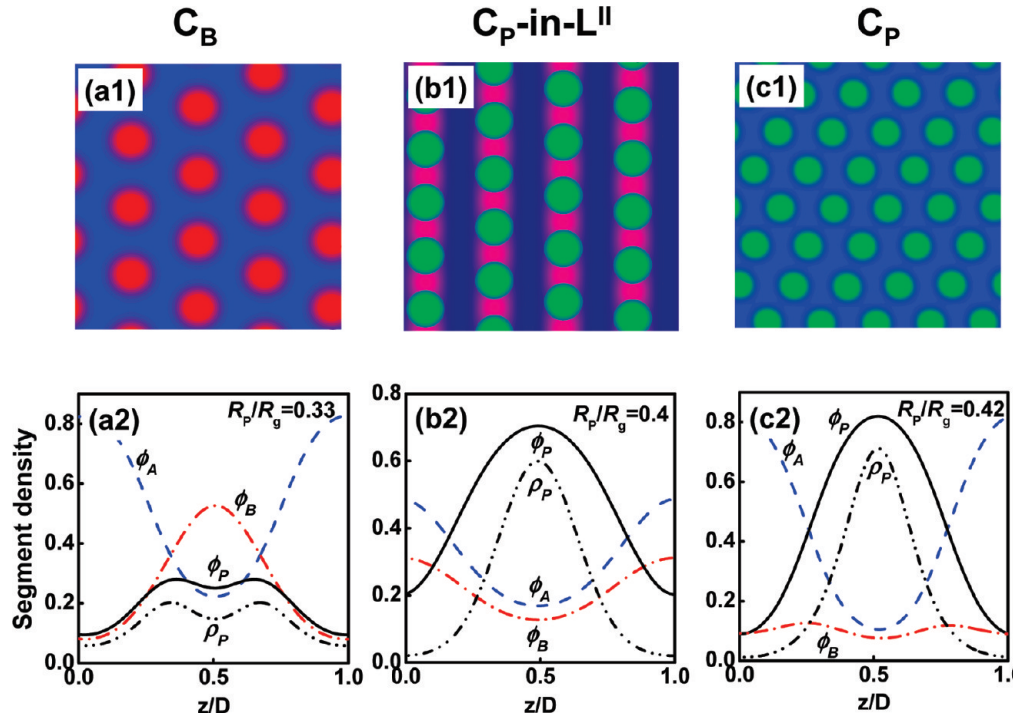

Figure 5. Various types of morphologies formed by ABP macromolecules at fixed A block volume fraction $f_A = 0.8$ with various particle radius: (a1) hexagonally arranged cylindrical $\mathbf{C}_B$ phase at $R_P/R_g = 0.33$; (b1) hierarchical structure $\mathbf{C}_P$-in-$\mathbf{L}^{II}$ at $R_P/R_g = 0.4$; (c1) hexagonally arranged cylindrical $\mathbf{C}_P$ phase at $R_P/R_g = 0.42$. Correspondingly, one-dimensional density profiles of A blocks (ϕ_A), B blocks (ϕ_B), particles P (ϕ_P), and particle centers (ρ_P) are given in a2−c2, respectively.

blocks and P particles, while A blocks form the matrix. The phase separation of AB copolymer tethers directs the distribution of P nanoparticles into the polymeric matrix. The P particles and B blocks are confined in the same cylindrical domains due to the connection of P particles with the B blocks. As particles become larger, the interaction between particles and polymeric tethers becomes dominate and consequently $\mathbf{C}_P$-in-$\mathbf{L}^{II}$ structure appears (Figure 6b). If the polymer chain tethers an inorganic nanoparticle, an inorganic/organic hybrid hierarchical nanostructure thus can be obtained. Such kind of hybrid structure is an interesting finding in the present work, which may find important applications in designing and creating advanced functional materials. With further increase in R_P/R_g, the structure $\mathbf{C}_P$-in-$\mathbf{L}^{II}$ transforms into structure $\mathbf{C}_P$, as shown in Figure 6c.

On the basis of the calculations, we constructed the phase diagram in $R_P/R_g - f_A$ space, which is shown in Figure 7. Eight characteristic zones are included: disorder phase, $\mathbf{C}_A$, $\mathbf{C}_B$, $\mathbf{C}_P$, **Lam**, $\mathbf{C}_P$-in-**C**, $\mathbf{C}_P$-in-$\mathbf{L}^{I}$, and $\mathbf{C}_P$-in-$\mathbf{L}^{II}$. When the value of R_P/R_g is smaller, the phase transition is viewed from **Dis**→ $\mathbf{C}_A$ → **Lam** → $\mathbf{C}_B$ → **Dis** as the volume fraction f_A increases. When the value of R_P/R_g is greater, complex ordered structures emerge as the sequence of $\mathbf{C}_P$ → $\mathbf{C}_P$-in-**C** → $\mathbf{C}_P$-in-$\mathbf{L}^{I}$ → $\mathbf{C}_P$-in-$\mathbf{L}^{II}$ → $\mathbf{C}_P$ with increasing f_A value. In this transition, the large-length-

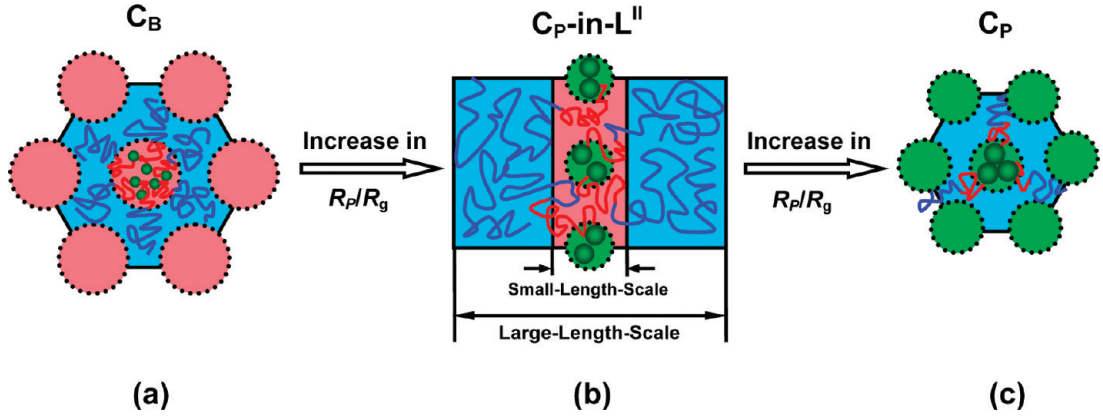

Figure 6. Schematic illustrations of (a) cylinder phase $\mathbf{C}_B$, (b) hierarchical structure $\mathbf{C}_P$-in-$\mathbf{L}^{II}$, and (c) cylindrical phase $\mathbf{C}_P$. The blue, red, and green regions, respectively, represent A block domains, B block domains, and nanoparticle P domains. The blue lines, red lines, and green spheres denote the A blocks, B blocks, and P nanoparticles, respectively.

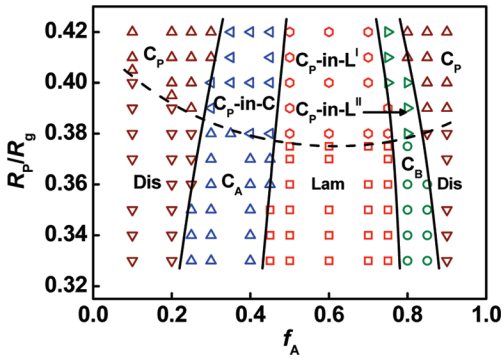

Figure 7. Phase diagram in $R_P/R_g - f_A$ space for ABP macromolecules with the interaction parameters $\chi_{AB}N = \chi_{AP}N = \chi_{BP}N = 30.0$. Dis labels the regions where the melt is disordered. The ordered regions include C_A (cylinders with minority domains formed by A blocks), Lam (lamellae), C_B (cylinders with minority domains formed by B blocks), C_P (cylinders with minority domains occupied nanoparticles), C_P-in-C (cylinders with cylinders at the interfaces), C_P-in-L^I (lamellae with cylinders at the interfaces), and C_P-in-L^{II} (lamellae with cylinders inside the domain). In this diagram, the phase boundaries are drawn to guide the eye based on the calculated points.

scale structure transforms from cylinder to lamella, then to cylinder, while the small-length-scale structure does correspondingly.

Some experimental evidence is available in the literature,[50] supporting our simulation results that polymer tethered nanoparticles can self-assemble into ordered structures and the phase behavior can be controlled by the particles size or content. Yockell-Lelièvre *et al.* connected the thiol end functionalized polystyrene chains to the gold nanoparticles *via* a two-step grafting-to method.[12] The resulting polymer tethered Au naoparticles self-organized into hexagonally ordered structure where the Au nanoparticle domains are distributed in the polymeric matrix of PS chains. Order→disorder transition in the studied samples occurs when the gold content becomes lower than approximately 0.5 vol %. Qualitatively compared with our SCFT calculations, hexagonally arranged nanoparticle arrays are observed (Figure 4a). This is in agreement with the experimental observations reported by Yockell-Lelièvre *et al.* The disordered morphology appears when the size of nanoparticles (associated with the volume fraction of particles) decreases, as shown in the phase diagram (Figure 7). The general features of the experiments are reproduced by our SCFT simulations, although several complex structures presented here are not observed in the experiments.

The above calculations were performed in a 2D lattice for solving the SCFT/DFT equations. With respect to 2D calculations, the 3D calculation may provide more detailed information regarding the nanostructures despite its computational difficulties. To have a deep insight into the ordered nanostructures, we carried out some 3D calculations on the present systems. All of the ordered nanostructures observed in the 2D calculations were reproduced in 3D space when the particle

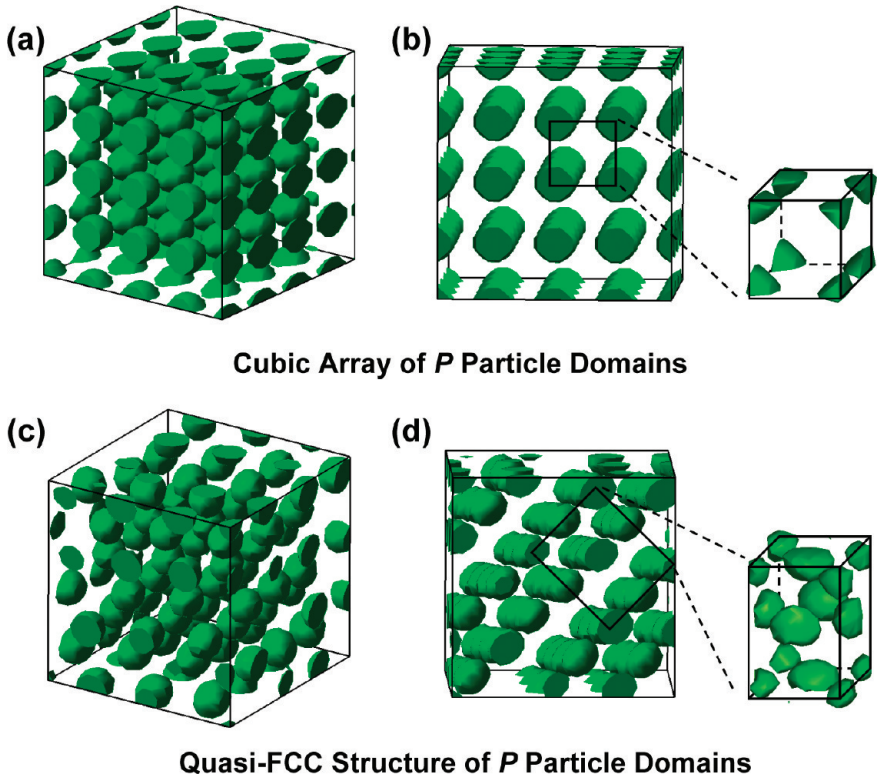

Figure 8. Three-dimensional density profiles of nanoparitles for $R_P/R_g = 0.45$ at different values of f_A: (a,b) cubic arrangements at $f_A = 0.26$; (c,d) quasi-fcc structure at $f_A = 0.6$. The enlarged domains show the unit cell of the cubic and quasi-fcc structures, respectively. The polymer tethers are not shown for clarity.

size R_P/R_g ranges from 0.32 to 0.43. The phase diagram obtained from 2D and 3D calculations is similar. However, we found that ABP molecules can self-assemble into a more diverse array of P particle domains for much larger particles (*e.g.*, $R_P/R_g = 0.45$). Figure 8 shows the density profiles for ABP macromolecules with larger particle size and different f_A. The profiles are presented in two different angles. When the composition of A blocks is smaller ($f_A = 0.26$), the spherical domains formed by P particles arranged cubically, as shown in Figure 8a,b (the polymer tethers, which are not phase-separated, occupy the space around the *P* particle domains). When $f_A = 0.6$, as shown in Figure 8c,d, AB polymeric tethers phase-separate to form the alternating lamellar phase, which exists like that shown in Figure 4c (it is not presented again in Figure 8). The spherical domains formed by P are packed in a sheet form within the lamellar plane formed by B blocks, constructing the large-length-scale structure, while in the small-length-scale, the P particle domains are arranged hexagonally. Regarding the arrangements of the P particle domains in the whole structure, they assume a fcc packing motif, as clearly viewed from the enlarged cell in Figure 8d. However, the fcc lattice cell is elongated along the direction normal to the plane of lamellae because of the asymmetric filling of AB polymeric tethers. Therefore, in a more appropriate representation, this lattice cell is a quasi-fcc rather than a perfect fcc. In the case of sufficiently small nanoparticles, the AB diblock copolymer tethers dominate the trend of phase transition, which behave like a pure diblock copolymer system. BCC, cylinder, lamella, and other structures can be formed with nanoparticles distributed in the polymeric domains.

In this work, we found that ABP macromolecules can self-assemble into ordered hierarchical nanostructures. If the tethered nanoparticles are inorganic, organic/inorganic hybrid hierarchal nanostructures can be obtained. Compared with the bulk copolymer system, such hybrid materials of copolymers and nanoparticles may significantly improve their mechanical, electronic, and photonic properties. The hierarchal structure may exhibit unique properties. As shown above, the organic polymeric A blocks and BP blocks self-assemble into the large-length-scale ordered structure, while inorganic nanoparticles and B blocks form the small-length-scale ordered structure. Each scale structure can contribute a distinct function to yield an integrated and multifunctional material like the natural organic/inorganic composites of bone and abalone nacre. A challenge for further studies is to create more complicated hierarchically ordered nanocomposites inspired by the biological systems.[51] The results obtained from the present work provide a promising strategy for producing a wide range of nanoscale structures, which can be of practical significance for applications in biomaterials and advanced functional materials.

CONCLUSIONS

In summary, we applied the SCFT/DFT method to study the phase behavior of ABP macromolecules, which are formed by attaching a flexible diblock copolymer chain to a nanoscopic spherical particle. For the chemically neutral nanoparticles, microphase separation of AB copolymer tethers directs the nanoparticle self-assembly into the ordered nanostructures. For the unlikable nanoparticles, ordered hierarchical structures are observed, such as cylinders with cylinders at the interfaces ($\mathbf{C}_P$-in-**C**), lamellae with cylinders at the interfaces ($\mathbf{C}_P$-in-$\mathbf{L}^{\mathbf{I}}$), and lamellae with cylinders inside a domain ($\mathbf{C}_P$-in-$\mathbf{L}^{\mathbf{II}}$). In these nanostructures, the large-length-scale structures are produced by the phase separation between the A blocks and BP blocks, whereas the small-length-scale structures are formed by the nanoparticles and B blocks. For both cases, the A block volume fraction f_A and the size of nanoparticles R_P/R_g affect the phase behaviors of ABP macromolecules significantly. We present the phase diagram in the parameter space of $R_P/R_g - f_A$ to show the relations between the resulting structures and these parameters. In addition, we found cubic arrays and quasi-fcc structures of P particle domains when 3D calculations were applied. For the hierarchical structures formed by ABP macromolecules, when the connected particles are inorganic nanoparticles, organic/inorganic hybrid hierarchical nanostructures can be obtained. The findings gained through the present work may find important applications in designing and creating advanced functional materials and biomaterials.

METHODS

To simulate the self-assembly behavior of the ABP macromolecules, we use the SCFT/DFT technique developed by Lee *et al.*,[48] which is appropriate for investigating the phase behaviors of the polymer grafted nanoparticles. The integrated SCFT/DFT approach identifies intriguing self-assembly morphologies of the diblock copolymers tethered nanoparticles. A powerful feature of this method is that *a priori* assumption about the morphology and the distribution of particles is not necessary.

In the framework of the SCFT/DFT approach, the free energy F (in units of k_BT) for per ABP macromolecule is given by[46,48]

$$F = -\ln\left(\frac{Q}{V}\right) + \frac{1}{V}\int d\mathbf{r}[\chi_{AB}N\phi_A(\mathbf{r})\phi_B(\mathbf{r}) + \chi_{AP}N\phi_A(\mathbf{r})\phi_P(\mathbf{r}) + \chi_{BP}N\phi_B(\mathbf{r})\phi_P(\mathbf{r}) - \omega_A(\mathbf{r})\phi_A(\mathbf{r}) - \omega_B(\mathbf{r})\phi_B(\mathbf{r}) - \omega_P(\mathbf{r})\rho_P(\mathbf{r}) - \xi(\mathbf{r})(1 - \phi_A(\mathbf{r}) - \phi_B(\mathbf{r}) - \phi_P(\mathbf{r})) + \rho_P(\mathbf{r})\psi_{HS}(\bar{\phi}_P(\mathbf{r}))] \quad (1)$$

Here, $\phi_A(\mathbf{r})$, $\phi_B(\mathbf{r})$, and $\phi_P(\mathbf{r})$ are the local volume fractions of A block, B block, and P particle, respectively; $\xi(\mathbf{r})$ is a Lagrange multiplier field invoked by the compressibility condition. χ_{ij} (i, j = A, B, P) characterizes the interaction between species i and j;

$\rho_P(\mathbf{r})$ is the particle center distribution. The local particle volume fraction $\phi_P(\mathbf{r})$ is given by

$$\phi_P(\mathbf{r}) = \frac{1-f}{v_R}\int_{|\mathbf{r}'|<R_P} d\mathbf{r}'\rho_P(\mathbf{r}'+\mathbf{r}) \quad (2)$$

Q is the partition function for a single ABP macromolecule chain given by

$$Q = \int d\mathbf{r} q(\mathbf{r},s)q^\dagger(\mathbf{r},s) \quad (3)$$

subjects to the effective chemical potential fields $\omega_A(\mathbf{r})$, $\omega_B(\mathbf{r})$, and $\omega_P(\mathbf{r})$. The contour length s increases continuously from 0 to f as the segment changes from one end to the other. The spatial coordinate $\mathbf{r}$ is in units of R_g; $q(\mathbf{r},s)$ is the propagator representing the probabilities of finding segments s at position $\mathbf{r}$, which satisfies the modified diffusion equations:

$$\frac{\partial}{\partial s}q(\mathbf{r},s) = (\nabla^2 - \omega_i(\mathbf{r}))q(\mathbf{r},s) \;\; \omega_i(\mathbf{r}) = \begin{cases}\omega_A(\mathbf{r}) & 0 \le s < f_A f \\ \omega_B(\mathbf{r}) & f_A f \le s < f\end{cases} \quad (4)$$

subject to the initial condition $q(\mathbf{r},0) = 1$. The backward propagator $q^\dagger(\mathbf{r},s)$ satisfies eq 4, subject to the initial condition $q^\dagger(\mathbf{r},f) = \int d\hat{\mathbf{n}}\exp(-w_P(\mathbf{r}+R_P\hat{\mathbf{n}}))$, where the unit vector $\hat{\mathbf{n}}$ is introduced to indicate the direction between the end of the coil polymer tether, which is attached to the surface of the particle, and the center of the nanoparticle P. The last term of eq 1 describes the steric energy of the particles according to Carnahan−Starling function[52,53]

$$\psi_{HS}(x) = \frac{4x - 3x^2}{(1-x)^2} \quad (5)$$

with the weighted nonlocal volume fraction $\bar{\phi}_P(\mathbf{r})$ of particles

$$\bar{\phi}_P(r) = \frac{1-f}{v_{2R}}\int_{|\mathbf{r}'|<2R_P} d\mathbf{r}'\rho_P(\mathbf{r}'+\mathbf{r}) \quad (6)$$

where v_{2R} is the volume of a sphere with radius $2R_P$.

Minimizing the free energy of eq 1 with respect to $\omega_A(\mathbf{r})$, $\omega_B(\mathbf{r})$, $\omega_P(\mathbf{r})$, $\phi_A(\mathbf{r})$, $\phi_B(\mathbf{r})$, $\rho_P(\mathbf{r})$, and $\xi(\mathbf{r})$ can lead to the following mean-field equations:

$$\phi_A(\mathbf{r}) = \frac{V}{Q}\int_0^{f_A f} ds q(\mathbf{r},s)q^\dagger(\mathbf{r},s) \quad (7)$$

$$\phi_B(\mathbf{r}) = \frac{V}{Q}\int_{f_A f}^{f} ds q(\mathbf{r},s)q^\dagger(\mathbf{r},s) \quad (8)$$

$$\rho_P(\mathbf{r}) = \frac{V}{Q}\exp(-\omega_P(\mathbf{r}))\int d\hat{\mathbf{n}} q(\mathbf{r}+R_P\hat{\mathbf{n}},f) \quad (9)$$

$$\omega_A(\mathbf{r}) = \chi_{AB}N\phi_B(\mathbf{r}) + \chi_{AP}N\phi_P(\mathbf{r}) + \xi(\mathbf{r}) \quad (10)$$

$$\omega_B(\mathbf{r}) = \chi_{AB}N\phi_A(\mathbf{r}) + \chi_{BP}N\phi_P(\mathbf{r}) + \xi(\mathbf{r}) \quad (11)$$

$$\omega_P(\mathbf{r}) = \psi_{HS}(\bar{\phi}_P(\mathbf{r})) + \frac{1-f}{v_{2R}}\int_{|\mathbf{r}'|<2R_P} d\mathbf{r}'\rho_P(\mathbf{r}'+\mathbf{r})\psi'(\bar{\phi}_P(\mathbf{r}'+\mathbf{r})) + \frac{1-f}{v_R}\int_{|\mathbf{r}'|<R_P} d\mathbf{r}'[\chi_{AP}N\phi_A(\mathbf{r}'+\mathbf{r}) + \chi_{BP}N\phi_B(\mathbf{r}'+\mathbf{r}) + \xi(\mathbf{r}'+\mathbf{r})] \quad (12)$$

where

$$\psi'_{HS}(x) = \frac{d\psi_{HS}(x)}{dx}$$

$$\phi_A(\mathbf{r}) + \phi_B(\mathbf{r}) + \phi_P(\mathbf{r}) = 1 \quad (13)$$

To numerically solve the SCFT equations, we implemented the combinatorial screening technique developed by Drolet and Fredrickson.[37] The calculation starts from the initial random density fields $\phi_A(\mathbf{r})$ and $\phi_B(\mathbf{r})$, which satisfy the Gaussian distribution. According to the strategy adopted by Balazs *et al.*, the initial distribution of particle centers is uniform, which allows us to find $\phi_P(\mathbf{r})$ and $\bar{\phi}_P(\mathbf{r})$ from eqs 2 and 6. The initial fields $\omega_A(\mathbf{r})$, $\omega_B(\mathbf{r})$, and $\omega_P(\mathbf{r})$ are calculated by eqs 10−12 (the initial incompressibility field $\xi(\mathbf{r})$ is set to be zero). The propagators $q(\mathbf{r},s)$ and $q^\dagger(\mathbf{r},s)$ can be obtained with the A and B fields and together with the particle field, and the single chain partition function Q can be found from eq 3. Next, the volume fractions are evaluated by eqs 2 and 7−9. To ensure the incompressibility of the system, the effective pressure field $\xi(\mathbf{r})$ is obtained by solving eqs 10, 11, and 13. Finally, the fields $\omega_A(\mathbf{r})$, $\omega_B(\mathbf{r})$, $\omega_P(\mathbf{r})$, and $\xi(\mathbf{r})$ are updated by means of a two-step Anderson mixing scheme.[54,55] The simulations were carried out until the free energy difference between two iterations is smaller than 10^{-5} and the incompressibility condition was achieved. In calculations, the simulations were mainly performed in two dimensions on a 128 × 128 lattice with periodic boundary conditions. To have a deep insight into the nanostructures, we also performed several calculations in three dimensions (48 × 48 × 48 lattice). To ensure that the observed morphologies are stable, we minimize our free energy with respect to the size of the simulation box, as proposed by Bohbot-Ravivv and Wang.[56]

Acknowledgment. This work was supported by National Natural Science Foundation of China (50925308). Support from Projects of Shanghai Municipality (09XD1401400, 0952 nm05100, 08DZ2230500, and B502) is also appreciated.

REFERENCES AND NOTES

1. Haes, A. J.; Van Duyne, R. P. A Nanoscale Optical Biosensor: Sensitivity and Selectivity of an Approach Based on the Localized Surface Plasmon Resonance Spectroscopy of Triangular Silver Nanoparticles. *J. Am. Chem. Soc.* **2002**, *124*, 10596–10604.
2. Arico, A. S.; Bruce, B.; Scrosati, B.; Tarascon, J. M.; van Schalkwijk, W. Nanostructured Materials for Advanced Energy Conversion and Storage Devices. *Nat. Mater.* **2005**, *4*, 366–377.
3. Maier, S. A.; Kik, P. G.; Atwater, H. A.; Melzter, S.; Harel, E.; Koel, B. E.; Requicha, A. A. G. Local Detection of Electromagnetic Energy Transport below the Diffraction Limit in Metal Nanoparticle Plasmon Waveguides. *Nat. Mater.* **2003**, *2*, 229–232.
4. Velev, O. D.; Tessier, P. M.; Lenhoff, A. M.; Kaler, E. W. Materials: A Class of Porous Metallic Nanostructures. *Nature* **1999**, *401*, 548.
5. Bockstaller, M. R.; Lapetnikov, Y.; Margel, S.; Thomas, E. L. Size-Selective Organization of Enthalpic Compatibilized Nanocrystals in Ternary Block Copolymer/Particle Mixtures. *J. Am. Chem. Soc.* **2003**, *125*, 5276–5277.
6. Yeh, S.-W.; Wei, K.-H.; Sun, Y.-S.; Jeng, U.-S.; Liang, K. S. Morphological Transformation of PS-b-PEO Diblock Copolymer by Selectively Dispersed Colloidal CdS Quantum Dots. *Macromolecules* **2003**, *36*, 7903–7907.
7. Lauter-Pasyuk, V.; Lauter, H. J.; Gordeev, G. P.; Müller-Buschbaum, P.; Toperverg, B. P.; Jernenkov, M.; Petry, W. Nanoparticles in Block-Copolymer Films Studied by Specular and Off-Specular Neutron Scattering. *Langmuir* **2003**, *19*, 7783–7788.
8. Lopes, W. A.; Jaeger, H. M. Hierarchical Self-Assembly of Metal Nanostructures on Diblock Copolymer Scaffolds. *Nature* **2001**, *414*, 735–738.
9. Zhang, L.; Lin, J. Hierarchically Ordered Nanocomposites Self-Assembled from Linear-Alternating Block Copolymer/Nanoparticle Mixture. *Macromolecules* **2009**, *42*, 1410–1414.
10. Zhang, Z.-L.; Horsch, M. A.; Lamm, M. H.; Glotzer, S. C. Tethered Nano Building Blocks: Toward a Conceptual Framework for Nanoparticle Self-Assembly. *Nano Lett.* **2003**, *3*, 1341–1346.
11. Glotzer, S. C. Some Assembly Required. *Science* **2004**, *306*, 419–420.

12. Yockell-Lelièvre, H.; Desbiens, J.; Ritcey, A. M. Two-Dimensional Self-Organization of Polystyrene-Capped Gold Nanoparticles. *Langmuir* **2007**, *23*, 2843–2850.
13. Schwaband, J. J.; Lichtenhan, J. D. Polyhedral Oligomeric Silsesquioxane(POSS)-Based Polymers. *Appl. Organomet. Chem.* **1998**, *12*, 707–713.
14. Laine, R. M.; Zhang, C.; Sellinger, A.; Viculis, L. Polyfunctional Cubic Silsesquioxanes as Building Blocks for Organic/Inorganic Hybrids. *Appl. Organomet. Chem.* **1998**, *12*, 715–723.
15. Drazkowski, D. B.; Lee, A.; Haddad, T. S. Morphology and Phase Transitions in Styrene-Butadiene-Styrene Triblock Copolymer Grafted with Isobutyl-Substituted Polyhedral Oligomeric Silsesquioxanes. *Macromolecules* **2007**, *40*, 2798–2805.
16. Chan, E. R.; Ho, L. C.; Glotzer, S. C. Computer Simulations of Block Copolymer Tethered Nanoparticle Self-Assembly. *J. Chem. Phys.* **2006**, *125*, 064905-1−064905-9.
17. Sknepnek, R.; Anderson, J. A.; Lamm, M. H.; Schmalian, J.; Travesset, A. Nanoparticle Ordering *via* Functionalized Block Copolymers in Solution. *ACS Nano* **2008**, *2*, 1259–1265.
18. Wang, Q.; Nealey, P. F.; de Pablob, J. J. Behavior of Single Nanoparticle/Homopolymer Chain in Ordered Structures of Diblock Copolymers. *J. Chem. Phys.* **2003**, *118*, 11278–11285.
19. Pryamitsyn, V.; Ganesan, V. Strong Segregation Theory of Block Copolymer-Nanoparticle Composites. *Macromolecules* **2006**, *39*, 8499–8510.
20. Alexeev, A.; Uspal, W. E.; Balazs, A. C. Harnessing Janus Nanoparticles to Create Controllable Pores in Membranes. *ACS Nano* **2008**, *2*, 1117–1122.
21. He, L.; Zhang, L.; Liang, H. The Effects of Nanoparticles on the Lamellar Phase Separation of Diblock Copolymers. *J. Phys. Chem. B* **2008**, *112*, 4194–4203.
22. Spontak, R. J.; Shankar, R.; Bowman, M. K.; Krishnan, A. S.; Hamersky, M. W.; Samseth, J.; Bockstaller, M. R.; Rasmussen, K. Ø. Selectivity- and Size-Induced Segregation of Molecular and Nanoscale Species in Microphase-Ordered Triblock Copolymers. *Nano Lett.* **2006**, *6*, 2115–2120.
23. Reister, E.; Fredrickson, G. H. Phase Behavior of a Blend of Polymer-Tethered Nanoparticles with Diblock Copolymers. *J. Chem. Phys.* **2005**, *123*, 214903-1–214903-13.
24. Yu, B.; Jin, Q.; Ding, D; Li, B.; Shi, A.-C. Confinement-Induced Morphologies of Cylinder-Forming Asymmetric Diblock Copolymers. *Macromolecules* **2008**, *41*, 4042–4054.
25. Guo, Z.; Zhang, G.; Qiu, F.; Zhang, H.; Yang, Y.; Shi, A.-C. Discovering Ordered Phases of Block Copolymers: New Results from a Generic Fourier-Space Approach. *Phys. Rev. Lett.* **2008**, *101*, 028301-1−028301-4.
26. Zhang, L.; Lin, J.; Lin, S. Morphologies and Bridging Properties of Graft Copolymers. *J. Phys. Chem B* **2007**, *111*, 351–357.
27. Zhang, L.; Lin, J.; Lin, S. Elastic Properties of Graft Copolymers in the Lamellar Phase Studied by Self-Consistent Field Theory. *Soft Matter* **2009**, *5*, 173–181.
28. Kim, J. U.; O'Shaughnessy, B. Nanoinclusions in Dry Polymer Brushes. *Macromolecules* **2006**, *39*, 413–425.
29. Kim, J. U.; Matsen, M. W. Interaction between Polymer-Grafted Particles. *Macromolecules* **2008**, *41*, 4435–4443.
30. Kim, J. U.; Matsen, M. W. Positioning Janus Nanoparticles in Block Copolymer Scaffolds. *Phys. Rev. Lett.* **2009**, *102*, 078303-1−078303-4.
31. Sides, S. W.; Kim, B. J.; Kramer, E. J.; Fredrickson, G. H. Hybrid Particle-Field Simulations of Polymer Nanocomposites. *Phys. Rev. Lett.* **2006**, *96*, 250601-1–250601-4.
32. Iacovella, C. R.; Horsch, M. A.; Zhang, Z.; Glotzer, S. C. Phase Diagrams of Self-Assembled Mono-Tethered Nanospheres from Molecular Simulation and Comparison to Surfactants. *Langmuir* **2005**, *21*, 9488–9494.
33. Zhang, X.; Chan, E. R.; Glotzer, S. C. Self-assembled Morphologies of Monotethered Polyhedral Oligomeric Silsesquioxane Nanocubes from Computer Simulation. *J. Chem. Phys.* **2005**, *123*, 184718-1–184718-6.
34. Horsch, M. A.; Zhang, Z.; Glotzer, S. C. Simulation Studies of Self-Assembly of End-Tethered Nanorods in Solution and Role of Rod Aspect Ratio and Tether Length. *J. Chem. Phys.* **2006**, *125*, 184903-1–184903-12.
35. Jayaraman, A.; Schweizer, K. S. Structure and Assembly of Dense Solutions and Melts of Single Tethered Nanoparticles. *J. Chem. Phys.* **2008**, *128*, 164904-1–164904-13.
36. Jayaraman, A.; Schweizer, K. S. Effect of the Number and Placement of Polymer Tethers on the Structure of Concentrated Solutions and Melts of Hybrid Nanoparticles. *Langmuir* **2008**, *24*, 11119–11130.
37. Drolet, F.; Fredrickson, G. H. Combinatorial Screening of Complex Block Copolymer Assembly with Self-Consistent Field Theory. *Phys. Rev. Lett.* **1999**, *83*, 4317–4320.
38. Fredrickson, G. H. *The Equilibrium Theory of Inhomogeneous Polymers*; Oxford University Press: Oxford, U.K., 2006.
39. Cochran, E. W.; Garcia-Cervera, C. J.; Fredrickson, G. H. Stability of the Gyroid Phase in Diblock Copolymers at Strong Segregation. *Macromolecules* **2006**, *39*, 2449–2451.
40. Ganesan, V.; Fredrickson, G. H. Field-Theoretic Polymer Simulations. *Europhys. Lett.* **2001**, *55*, 814–820.
41. Drolet, F.; Fredrickson, G. H. Optimizing Chain Bridging in Complex Block Copolymers. *Macromolecules* **2001**, *34*, 5317–5324.
42. Ye, X.; Shi, T.; Lu, Z.; Zhang, C.; Sun, Z.; An, L. Study of Morphology and Phase Diagram of π-Shaped ABC Block Copolymers Using Self-Consistent-Field Theory. *Macromolecules* **2005**, *38*, 8853–8857.
43. Chen, J.; Sun, Z.; Zhang, C.; An, L.; Tong, Z. Self-Assembly of Rod-Coil-Rod ABA-type Triblock Copolymers. *J. Chem. Phys.* **2008**, *128*, 074904-1−074904-6.
44. Thompson, R. B.; Ginzburg, V. V.; Matsen, M. W.; Balazs, A. C. Predicting the Mesophases of Copolymer-Nanoparticle Composites. *Science* **2001**, *292*, 2469–2472.
45. Zhou, L.; Ma, Y. Phase Behavior of Nanoparticle-Copolymer Films Confined Between Polymer-Grafted Surfaces. *J. Phys.: Condens. Matter* **2008**, *20*, 095006-1−095006-5.
46. Lee, J. Y.; Thompson, R. B.; Jasnow, D.; Balazs, A. C. Effect of Nanoscopic Particles on the Mesophase Structure of Diblock Copolymers. *Macromelcules* **2002**, *35*, 4855–4858.
47. Lee, J. Y.; Shou, Z.; Balazs, A. C. Modeling the Self-Assembly of Copolymer-Nanoparticle Mixtures Confined between Solid Surfaces. *Phys. Rev. Lett.* **2003**, *91*, 136103-1–136103-4.
48. Lee, J. Y.; Balazs, A. C.; Thompson, R. B.; Hill, R. M. Self-Assembly of Amphiphilic Nanoparticle-Coil "Tadpole" Macromolecules. *Macromolecules* **2004**, *37*, 3536–3539.
49. Zhang, L.; Lin, J.; Lin, S. Self-Assembly Behavior of Amphiphilic Block Copolymer/Nanoparticle Mixture in Dilute Solution Studied by Self-Consistent-Field Theory/Density Functional Theory. *Macromolecules* **2007**, *40*, 5582–5592.
50. Claridge, S. A.; Jr, A. W. C.; Khanna, S. N.; Murray, C. B.; Sen, A.; Weiss, P. S. Cluster-Assembled Materials. *ACS Nano* **2009**, *3*, 244–255.
51. Vaia, R.; Baur, J. Adaptive Composites. *Science* **2008**, *319*, 420–421.
52. Carnahan, N. F.; Starling, K. E. Equation of State for Nonattracting Rigid Spheres. *J. Chem. Phys.* **1969**, *51*, 635–636.
53. Tarazona, P. A Density Functional Theory of Melting. *Mol. Phys.* **1984**, *52*, 81–96.
54. Eyert, V. A Comparative Study on Methods for Convergence Acceleration of Iterative Vector Sequences. *J. Comput. Phys.* **1996**, *124*, 271–285.
55. Thompson, R. B.; Rasmussen, K.Ø.; Lookma, T. Improved Convergence in Block Copolymer Self-Consistent Field Theory by Anderson Mixing. *J. Chem. Phys.* **2004**, *120*, 31–34.
56. Bohbot-Raviv, Y.; Wang, Z.-G. Combinatorial Screening of Complex Block Copolymer Assembly with Self-Consistent Field Theory. *Phys. Rev. Lett.* **1999**, *83*, 4317–4320.